Higher-Order Sinusoidal-Input Describing Function Analysis for a Class of Multiple-Input Multiple-Output Convergent Systems

Eijk, Luke F.van; Kostic, Dragan; Khosravi, Mohammad; HosseinNia, S. Hassan

DOI
10.1109/TAC.2024.3442877

Publication date
2025

Document Version
Final published version

Published in
IEEE Transactions on Automatic Control

Citation (APA)
Eijk, L. F. V., Kostic, D., Khosravi, M., & HosseinNia, S. H. (2025). Higher-Order Sinusoidal-Input Describing Function Analysis for a Class of Multiple-Input Multiple-Output Convergent Systems. *IEEE Transactions on Automatic Control*, *70*(1), 673-680. https://doi.org/10.1109/TAC.2024.3442877

Higher Order Sinusoidal-Input Describing Function Analysis for a Class of Multiple-Input Multiple-Output Convergent Systems

Luke F. van Eijk, Dragan Kostić, Mohammad Khosravi, and S. Hassan HosseinNia, *Senior Member, IEEE*

***Abstract*—This article introduces output prediction methods for two types of systems containing sinusoidal-input uniformly convergent (SIUC) elements. The first method considers these elements in combination with single-input single-output linear time-invariant (LTI) systems before, after, and in parallel to them. The second method considers a multiple-input multiple-output LTI system where each input is controlled by an SIUC element. The output prediction only requires frequency-response functions of the LTI elements and is fully accurate for sinusoidal inputs.**

***Index Terms*—Frequency domain, higher order sinusoidal-input-describing function (HOSIDF), multiple-input multiple-output (MIMO) systems, uniformly convergent systems.**

I. Introduction

LINEAR time-invariant (LTI) control has played an important role in shaping the modern world [1]. It has especially proven to be effective in controlling LTI plants, because closed-loop performance of the complete system can be analyzed without the need to develop a parametric plant model. Instead, a frequency-response function (FRF) can be utilized [2], which can be obtained based purely on measurement data. Advanced system identification methods have been developed to identify a highly accurate FRF with only a limited amount of measurement data [3]. With this FRF, as well as a given LTI controller, closed-loop system performance can be straightforwardly evaluated using, e.g., Bode plots, such as sensitivity functions [2], which is even possible for general multiple-input multiple-output (MIMO) LTI systems. Therefore, this allows the user to intuitively redesign the controller in order to obtain more desirable closed-loop behavior, also known as loop-shaping.

Even though the LTI control regime has enabled numerous technological advancements, ever-growing system demands make it increasingly difficult for LTI control to meet the desired performance specifications. This is caused by the fact that LTI control suffers from inherent limitations, such as Bode's gain–phase relationship and Bode's sensitivity integral [4]. For control practitioners, this typically means that they are faced with a tradeoff between speed, accuracy, and robustness of the system. Loosely speaking, improving one of them will result in a worsening of (at least one of) the others.

A logical step toward overcoming the inherent limitations of LTI control is moving to nonlinear time-invariant (NLTI) control strategies. It has been analytically shown in the literature that certain NLTI control elements are able to overcome inherent limitations of LTI control, such as the hybrid integrator-gain system (HIGS) [5], as well as certain types of variable gain control (VGC) [6] and reset control [7]. However, intuitively assessing closed-loop performance for these (and many other) NLTI control strategies based on a nonparametric plant model is less trivial. Namely, the possibility to create Bode plots of LTI control systems is driven by the fact that providing a sinusoidal input to an LTI system results in a sinusoidal output. This does not hold for general NLTI systems.

A tool that is often utilized for FRF-based closed-loop performance analysis of control systems containing NLTI elements, such as HIGS [8], [9], VGC [10], and reset control [11], is the sinusoidal-input describing function (SIDF) method [12]. In essence, this method can be utilized for any NLTI element that, provided a sinusoidal input, uniformly converges to a periodic output with the same period as the input sinusoid. When these types of systems are provided with a sinusoidal input, their output signal can be modeled as a Fourier series, containing not only the harmonic of the input sinusoid, but also higher order harmonics of it (and potentially a constant offset). In the SIDF method, the effect of the higher order harmonics is neglected, and it is assumed that the output of the NLTI element only consists of the first harmonic. Subsequently, closed-loop performance can be intuitively assessed using Bode plots, based purely on the first harmonic of the NLTI elements and FRFs of other (potentially MIMO) LTI elements that are in the loop. However, since the SIDF method only provides an approximation of the NLTI elements' behavior, one can imagine that the predicted closed-loop performance can be inaccurate, see, e.g., [13].

In order to obtain more accurate closed-loop performance predictions compared to the SIDF-method, it is first necessary to obtain an accurate representation of the open-loop system performance. A crucial step toward this goal are the works in [14] and [15, Ch. 2], where the higher order SIDF (HOSIDF) method is developed. This method allows to analytically compute the output signal of a sinusoidal-input uniformly convergent system—provided a sinusoidal input—with full accuracy, taking the effect of all the higher order harmonics into account. By means of the HOSIDF method, one can also visualize the behavior of each harmonic in the frequency domain. The HOSIDF method has proven itself as an intuitive tool for redesigning certain types of nonlinear controllers in order to obtain desired closed-loop behaviour, as shown in [13] for reset controllers, and in [16], for HIGS-based controllers.

However, the open loop does usually not only consists of a sinusoidal-input uniformly convergent element, but also contains LTI

Manuscript received 9 April 2024; revised 1 July 2024; accepted 8 August 2024. Date of publication 13 August 2024; date of current version 31 December 2024. This work was supported by ASMPT. Recommended by Associate Editor L. B. Freidovich. *(Corresponding author: Luke F. van Eijk.)*

Luke F. van Eijk is with the Department of Precision and Microsystems Engineering, Delft University of Technology, 2628 CD Delft, The Netherlands, and also with ASMPT, 6641 TL Beuningen, The Netherlands (e-mail: L.F.vanEijk@tudelft.nl).

Dragan Kostić is with ASMPT, 6641 TL Beuningen, The Netherlands (e-mail: dragan.kostic@asmpt.com).

Mohammad Khosravi is with the Delft Center for Systems and Control, Delft University of Technology, 2628 CD Delft, The Netherlands (e-mail: Mohammad.Khosravi@tudelft.nl).

S. Hassan HosseinNia is with the Department of Precision and Microsystems Engineering, Delft University of Technology, 2628 CD Delft, The Netherlands (e-mail: S.H.HosseinNiaKani@tudelft.nl).

Digital Object Identifier 10.1109/TAC.2024.3442877

elements around it. A method for accurate output prediction of systems consisting of a static nonlinearity and a single-input single-output (SISO) LTI postfilter is given in [12, Ch. 3], even prior to the development of the HOSIDF method in [15, Ch. 2]. In [17], the same has been done for systems with multiple parallel lines containing a static polynomial nonlinearity and SISO LTI prefilters and postfilters. In the same work, an explicit expression for the HOSIDFs is given, allowing for an intuitive frequency-domain analysis. The HOSIDF-method has also been extended for two types of dynamic nonlinearities. The first being reset controllers, for which the effect of SISO LTI postfilters is investigated in [13]. Several works have also attempted to extend the HOSIDF method for reset controllers by including the effect of SISO LTI prefilters, such as [18], [19], and [20]. However, these only give the correct magnitude of the HOSIDFs and not its phases, hence not allowing for a correct output prediction. The second dynamic nonlinearity is HIGS, for which the HOSIDF method has been extended in [16] to include the effect of SISO LTI postfilters and parallel filters. To the best of the author's knowledge, the HOSIDF method has thus far not been extended toward MIMO control systems. It is however interesting to note that, in [21], a method has been developed that allows for an accurate output prediction for systems with MIMO LTI plants controlled on each input by an ideal relay.

The aim of this work is to extend upon the existing literature related to the HOSIDF method by means of two contributions. As a first minor contribution, we show that the HOSIDF method for sinusoidal-input uniformly convergent elements, as developed in [15, Ch. 2], can be extended to include the effect of SISO LTI elements before, after, and in parallel to them. This result naturally covers all existing extensions that we discussed, except the one with multiple static polynomial nonlinearities. However, the developed HOSIDF method can also be utilized to study many other types of NLTI elements, as long as they are sinusoidal-input uniformly convergent. As the second and primary contributions, we extend the HOSIDF method toward MIMO LTI elements for which each input is controlled by a SISO sinusoidal-input uniformly convergent element.

The rest of this article is organized as follows. In Section II, the necessary preliminaries into the HOSIDF method are provided. Subsequently, the main results of this work are presented in Section III. In Section IV, two illustrative examples are given that illustrate the benefits of our work. Finally, Section V concludes this article.

II. Preliminaries

In this work, we deal with systems containing a SISO NLTI element that is *sinusoidal-input uniformly convergent*, which is surrounded by various LTI elements. The former element is uniformly convergent (see, e.g., [22, Def. 2.3]) for the class of sinusoidal inputs given by

$$r^0(t) = \hat{r}\sin(\omega t) \tag{1}$$

with amplitude $\hat{r} \in \mathbb{R}_{>0}$, excitation frequency $\omega \in \mathbb{R}_{>0}$, and time $t \in \mathbb{R}$. This means that—given a sinusoidal input—the element's output will (uniformly) converge to a stationary output $v_{\mathrm{s}}^0(t)$.

Remark 2.1: Note that there is a broad range of nonlinearities that are sinusoidal-input uniformly convergent. This property holds for all static nonlinearities, such as saturation, deadzone, ideal relays, and VGC. Furthermore, it holds for several dynamic nonlinearities, such as reset controllers and HIGS.

In the rest of this article, we assume that the sinusoidal-input uniformly convergent element satisfies Assumption 2.1, which we consider to be a mild assumption on control elements.

Assumption 2.1: The stationary output of the sinusoidal-input uniformly convergent element is a piecewise continuous periodic function with period $T = \frac{2\pi}{\omega}$.

As shown in [15, Ch. 2], when Assumption 2.1 holds, the stationary output of a sinusoidal-input uniformly convergent element can be described by the Fourier series

$$v_{\mathrm{s}}^0(t) = |H^0(\omega,\hat{r})|\hat{r} + \cdots \sum_{n=1}^{\infty} |H^n(\omega,\hat{r})|\hat{r}\sin\left(n\omega t + \angle H^n(\omega,\hat{r})\right) \tag{2}$$

with H^n the nth-order SIDF, $n \in \mathbb{N}$. Note that $H^0 \in \mathbb{R}$ and $H^n \in \mathbb{C}\forall\, n \neq 0$. Next, consider the case in which the element is subject to a time-shifted sinusoidal input $r(t) := r^0(t + \frac{\varphi_{\mathrm{r}}}{\omega})$, $\varphi_{\mathrm{r}} \in \mathbb{R}$, such that

$$r(t) = \hat{r}\sin(\omega t + \varphi_{\mathrm{r}}). \tag{3}$$

Since the nonlinear element is time-invariant, its output converges to a (time-shifted) solution $v(t) := v_{\mathrm{s}}^0(t + \frac{\varphi_{\mathrm{r}}}{\omega})$, such that

$$v(t) = |H^0(\omega,\hat{r})|\hat{r} + \cdots \sum_{n=1}^{\infty} |H^n(\omega,\hat{r})|\hat{r}\sin\left(n(\omega t + \varphi_{\mathrm{r}}) + \angle H^n(\omega,\hat{r})\right). \tag{4}$$

Visually, in the stationary case, one can think of such an element as a virtual harmonics expander (VHE) [15, Ch. 2], as portrayed in Fig. 1. When $k \in \mathbb{N}$ goes to infinity, one obtains the stationary output (4).

III. Main Results

Consider the SISO NLTI system K, as depicted in Fig. 2. SISO LTI system C_1 has signal $e \in \mathbb{R}$ as its input and r as its output. SISO NLTI system N has r as its input and v as its output. SISO LTI system C_2 has r as its input and $w \in \mathbb{R}$ as its output. Finally, SISO LTI system C_3 has $z := v + w$ as its input and $u \in \mathbb{R}$ as its output. Note that the input–output relations of C_1, C_2, and C_3, can be described in the frequency domain by

$$R(s) = C_1(s)E(s) \tag{5}$$

$$W(s) = C_2(s)R(s) \tag{6}$$

$$U(s) = C_3(s)Z(s) \tag{7}$$

respectively, where $s \in \mathbb{C}$ is the Laplace variable, and the capitalized variables $E, R, W, Z, U \in \mathbb{C}$ are the Laplace transforms of the respective noncapitalized time-domain signals. In Lemma 3.1, an analytical expression is presented to describe the stationary solution to which output u converges when the open-loop SISO NLTI system in Fig. 2 is subject to a sinusoidal input.

Lemma 3.1: Consider the system depicted in Fig. 2 with SISO LTI elements C_1, C_2, and C_3, and SISO NLTI element N, subject to a sinusoidal input

$$e(t) = \hat{e}\sin(\omega t + \varphi_{\mathrm{e}}) \tag{8}$$

with amplitude $\hat{e} \in \mathbb{R}_{>0}$ and phase $\varphi_{\mathrm{e}} \in \mathbb{R}$, and with any initial conditions for C_1, C_2, C_3, and N. Then, if LTI elements C_1, C_2, and C_3 are Hurwitz, NLTI element N is sinusoidal-input uniformly convergent, and Assumption 2.1 holds, the system's output converges to a unique $\frac{2\pi}{\omega}$-periodic solution

$$u(t) = |K^0(\omega,\hat{e})|\hat{e} + \cdots \sum_{n=1}^{\infty} |K^n(\omega,\hat{e})|\hat{e}\sin\left(n(\omega t + \varphi_{\mathrm{e}}) + \angle K^n(\omega,\hat{e})\right) \tag{9}$$

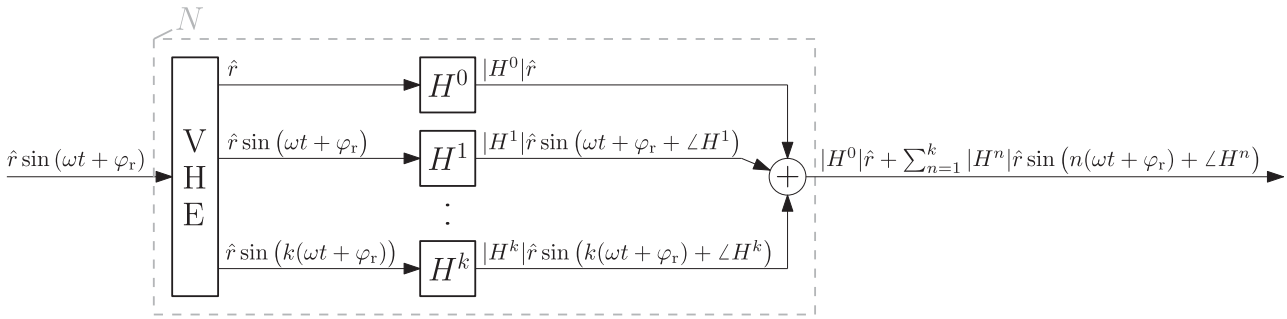

Fig. 1. Schematic representation of a SISO NLTI element N that is sinusoidal-input uniformly convergent, modeled as a VHE (adapted from [15]).

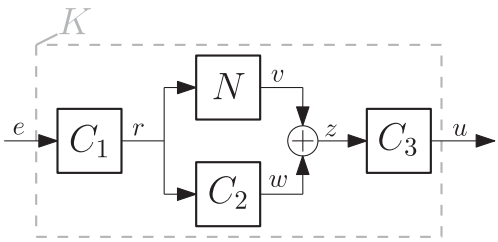

Fig. 2. Schematic representation of a SISO NLTI system K with SISO LTI elements C_1, C_2, and C_3, and SISO NLTI element N.

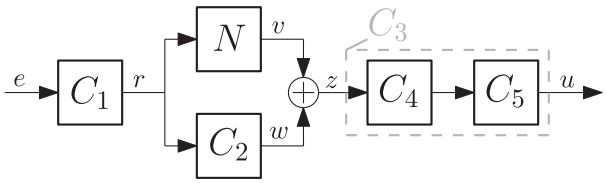

Fig. 3. Schematic representation of an NLTI system with SISO LTI elements C_1, C_2, C_4, and C_5, and SISO NLTI element N.

where the open-loop HOSIDFs are given by

$$K^n(\omega,\hat{e}) := \begin{cases} C_3(0)H^0(\omega,\hat{r})C_1(j\omega), & \text{for } n=0 \\ C_3(j\omega)\left[H^1(\omega,\hat{r})+C_2(j\omega)\right]C_1(j\omega) & \\ & \text{for } n=1 \\ C_3(nj\omega)H^n(\omega,\hat{r})C_1(j\omega)e^{j(n-1)\angle C_1(j\omega)} & \\ & \text{for } n>1 \end{cases} \tag{10}$$

$$\hat{r} = |C_1(j\omega)|\hat{e} \tag{11}$$

with an imaginary number $j := \sqrt{-1}$, H^n the nth-order SIDF of N, and C_1, C_2, and C_3 as in (5)–(7), respectively.

Proof: See Appendix A.

Several conclusions can be drawn from Lemma 3.1. First of all, the lemma provides an intuitive link between open-loop time-domain and frequency-domain behavior for the considered class of systems, by means of the HOSIDF method. This also allows to compute the time-domain solution based purely on the FRFs of the LTI elements, as well as the HOSIDFs of the sinusoidal-input uniformly convergent element. Second, note that any of the SISO LTI elements C_1, C_2, or C_3 in Fig. 2 can also consist of multiple cascaded SISO LTI elements. As an example, consider Fig. 3, where SISO LTI element C_3 contains a cascade of SISO LTI elements C_4 and C_5. Therefore, $C_3(s) = C_5(s)C_4(s)$ in (7), such that Lemma 3.1 can still be utilized. Third, when the conditions imposed in the lemma on all the elements hold, the entire system K inherits the property of being sinusoidal-input uniformly convergent and one can observe that the stationary output given in (9) satisfies Assumption 2.1. This observation eases the analysis of these types of systems, since it allows for abstracting away the SISO LTI elements. This intermediate step helps to simplify the proof of our next result.

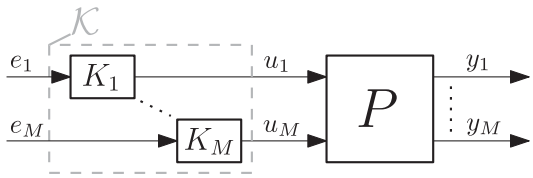

Fig. 4. Schematic representation of a MIMO LTI system P controlled by multiloop SISO NLTI system $\mathcal{K}$, containing multiple SISO NLTI elements K_i.

Remark 3.1: Note that LTI prefilter C_1 serves as a shaping filter for the input-amplitude $\hat{r}$ of the NLTI element N. It also serves as a shaping filter for the phase of the HOSIDFs. Even though shaping this phase does not change the root mean square value of the output signal (Parseval's theorem), it can change other characteristics of the signal, such as its maximum absolute value.

Next, consider the MIMO NLTI system depicted in Fig. 4, with MIMO LTI system P controlled by multiloop SISO NLTI system $\mathcal{K}$. The latter contains multiple SISO NLTI elements K_i, $i \in [1, M]$, $M \in \mathbb{N}$, such that element K_i has input $e_i \in \mathbb{R}$ and output $u_i \in \mathbb{R}$. Therefore, $e(t) = [e_1(t), \ldots, e_M(t)]^{\mathrm{T}}$ is the input to system $\mathcal{K}$, and $u(t) = [u_1(t), \ldots, u_M(t)]^{\mathrm{T}}$ is its output. We want to note again that each element K_i can contain a more complicated underlying system, such as the one in Fig. 3. System P takes u as its input and gives $y(t) = [y_1(t), \ldots, y_M(t)]^{\mathrm{T}}$ as the output. Note that system P can be described in the frequency domain by

$$Y(s) = P(s)U(s) \tag{12}$$

$$P(s) := \begin{bmatrix} P_{1,1}(s) & & P_{1,M}(s) \\ & \ddots & \\ P_{M,1}(s) & & P_{M,M}(s) \end{bmatrix} \tag{13}$$

where the capitalized variables U, $Y \in \mathbb{C}^{M\times 1}$ are the Laplace transforms of the respective noncapitalized time-domain signals, and $P_{j,i} \in \mathbb{C}$ is the transfer function from input u_i to output y_j, $j \in [1, M]$. In Theorem 3.1, an analytical expression is presented to describe the stationary solution to which output y converges when the system in Fig. 4 is subject to sinusoidal inputs in e.

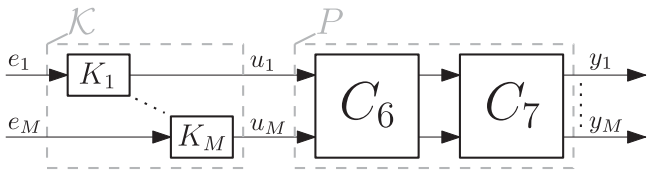

Fig. 5. Schematic representation of an open-loop NLTI system with MIMO LTI elements C_6 and C_7, and multiloop SISO NLTI element $\mathcal{K}$.

Theorem 3.1: Consider the system depicted in Fig. 4 with MIMO LTI system P and multiloop SISO NLTI system $\mathcal{K}$, subject to an input

$$e(t) = [\hat{e}_1 \sin(\omega_1 t + \varphi_{e,1}), \ldots, \hat{e}_M \sin(\omega_M t + \varphi_{e,M})]^{\mathrm{T}} \tag{14}$$

with excitation frequencies $\omega_i \in \mathbb{R}_{>0}$, input amplitudes $\hat{e}_i \in \mathbb{R}_{>0}$, input phases $\varphi_{e,i} \in \mathbb{R}$, and any initial conditions for system P and elements K_i. Then, if LTI system P is Hurwitz, all NLTI elements K_i are sinusoidal-input uniformly convergent, and Assumption 2.1 holds for all signals u_i, the system output converges to a unique solution, where

$$y_j(t) = \sum_{i=1}^{M} \Bigg[|L^0_{j,i}(\omega_i, \hat{e})| \hat{e}_i + \cdots \sum_{n=1}^{\infty} |L^n_{j,i}(\omega_i, \hat{e})| \hat{e}_i \sin\left(n(\omega_i t + \varphi_{e,i}) + \angle L^n_{j,i}(\omega_i, \hat{e})\right) \Bigg]. \tag{15}$$

Here, the MIMO open-loop HOSIDFs are given by

$$L^n(\omega, \hat{e}) := P(nj\omega)\mathcal{K}^n(\omega, \hat{e}) \tag{16}$$

$$\mathcal{K}^n(\omega, \hat{e}) := \begin{bmatrix} K_1^n(\omega, \hat{e}_1) & & 0 \\ & \ddots & \\ 0 & & K_M^n(\omega, \hat{e}_M) \end{bmatrix} \tag{17}$$

with excitation frequency $\omega \in \mathbb{R}_{>0}$, input amplitudes $\hat{e} = [\hat{e}_1, \ldots, \hat{e}_M]$, P as in (13), K_i^n the nth-order SIDF of K_i, and $L^n_{j,i}$ the matrix-entry of L^n in the jth row and ith column.

Proof: See Appendix B.

Several interesting conclusions can be drawn from Theorem 3.1. First of all, the theorem provides an intuitive link between open-loop time-domain and frequency-domain behavior for the considered class of systems, by means of the developed HOSIDF method. This also allows to compute the time-domain solution based purely on the FRF of the MIMO LTI system P, as well as the HOSIDFs of the sinusoidal-input uniformly convergent elements K_i. Second, note that MIMO LTI system P in Fig. 4 can also consist of multiple cascaded MIMO LTI systems. As an example, consider Fig. 5, where MIMO LTI system P contains a cascade of MIMO LTI elements C_6 and C_7. Therefore, $P(s) = C_7(s)C_6(s)$ in (12), such that Theorem 3.1 can still be utilized. In addition, any sinusoidal-input uniformly convergent element K_i can internally contain SISO LTI prefilters, postfilters, and parallel filters, since this again yields a sinusoidal-input uniformly convergent element according to Lemma 3.1. Third, the theorem allows for different types of sinusoidal-input uniformly convergent elements in one system. For example, one input of MIMO LTI system P can be controlled by a reset controller, whereas another input is being controlled by means of VGC. Finally, the theorem shows that the system output can still be predicted when multiple separate sinusoids are simultaneously applied to multiple inputs e_i, as in (14). Namely, in that case, the inputs to all of the nonlinear elements remain sinusoidal, hence, allowing a HOSIDF analysis.

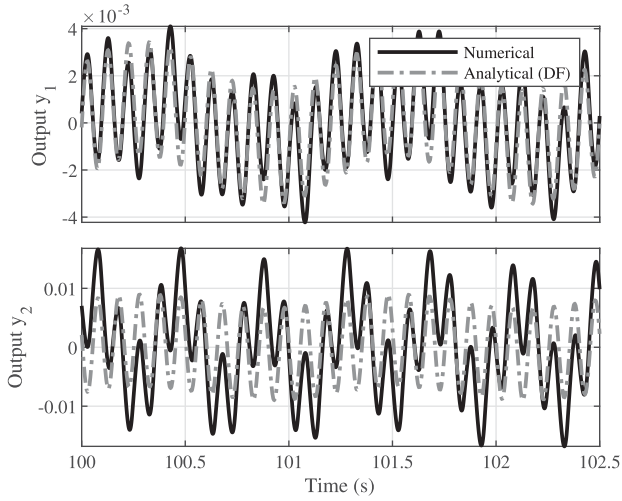

Fig. 6. Numerically computed system output compared to the analytical solution using the SIDF-method, for the considered example with P, K_1, and K_2, as in (18)–(20), and a sinusoidal input (21) with $\omega_1 = 0.81 \cdot 2\pi$, $\omega_2 = 10 \cdot 2\pi$, $\hat{e}_1 = 1$, $\hat{e}_2 = 10$, $\varphi_{e,1} = \frac{\pi}{4}$, and $\varphi_{e,2} = \frac{\pi}{8}$.

IV. Illustrative Example

Consider the case in which the double-input double-output LTI system P in Fig. 4 represents a double mass–spring–damper system, given in the frequency domain by

$$P(s) = \begin{bmatrix} m_{fs}s^2 + c_{fs}s + k_{fs} & -m_{fs}s^2 \\ c_{fs}s + k_{fs} & m_{cs}s^2 + c_{cs}s + k_{cs} \end{bmatrix} G^{-1}_{den}(s) \tag{18}$$

$$G_{den}(s) = (m_{fs}s^2 + c_{fs}s + k_{fs})\left(m_{cs}s^2 + \cdots (c_{fs} + c_{cs})s + k_{fs} + k_{cs}\right) - (c_{fs}s + k_{fs})^2 \tag{19}$$

where $m_{cs} = 2.34$, $c_{cs} = 17$, $k_{cs} = 2000$, $m_{fs} = 0.57$, $c_{fs} = 0.28$, and $k_{fs} = 146$. The parameter values are based on the one degree of freedom dual precision stage considered in [23]. The NLTI elements are both a Clegg integrator (CI) [24], given in state-space representation by

$$K_i := \begin{cases} \dot{x}_i(t) = \omega^i_{CI} e_i(t), & \text{if } e_i(t) \neq 0 \\ x_i(t^+) = 0, & \text{if } e_i(t) = 0 \\ u_i(t) = x_i(t) \end{cases} \tag{20}$$

with state $x_i \in \mathbb{R}$, $t^+ := \lim_{\tau \to t, \tau > t} \tau$, and integrator frequencies $\omega^1_{CI} = 2\pi$ and $\omega^2_{CI} = 10 \cdot 2\pi$. We now look at the case in which the system is subject to a sinusoidal input

$$e(t) = [\hat{e}_1 \sin(\omega_1 t + \varphi_{e,1}),\ \hat{e}_2 \sin(\omega_2 t + \varphi_{e,2})]^{\mathrm{T}} \tag{21}$$

where $\hat{e}_1 = 1$, $\hat{e}_2 = 10$, $\varphi_{e,1} = \frac{\pi}{4}$, and $\varphi_{e,2} = \frac{\pi}{8}$. In Sections IV-A and IV-B, we consider two examples in which different sets of input frequencies are used.

A. Example I: Nonnegligible Higher Order Harmonics

In this first example, we use the input frequencies $\omega_1 = 0.81 \cdot 2\pi$ and $\omega_2 = 10 \cdot 2\pi$. In Fig. 6, the system output is portrayed that is obtained from a numerical simulation, where the initial conditions are all set to zero.

When the SIDF-method is utilized to create a quasi-linear approximation of the NLTI elements, one can subsequently utilize LTI

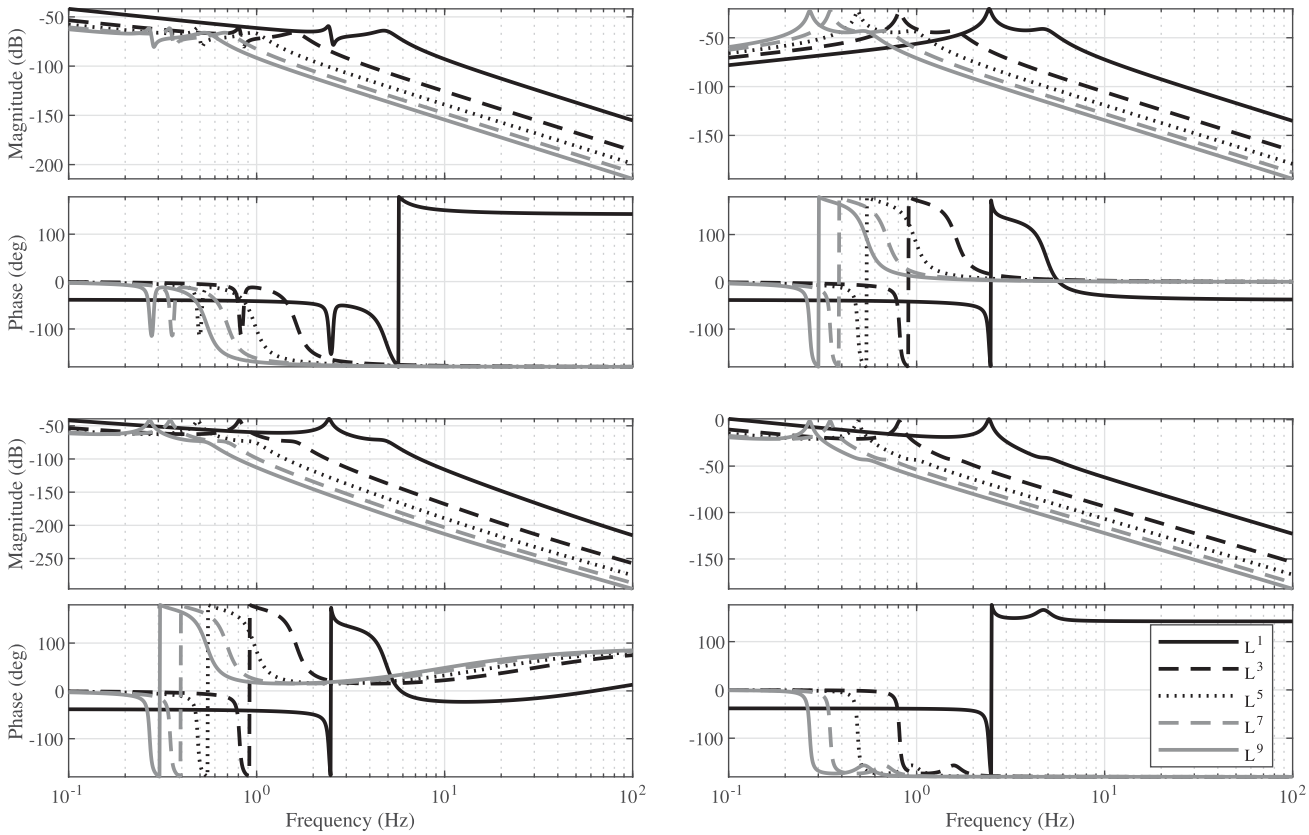

Fig. 7. Magnitude and phase characteristics of the MIMO open-loop HOSIDFs for the example system in (18)–(20), computed based on (16) and (17) in Theorem 3.1.

reasoning for MIMO systems [25]. In that case, the open-loop output can be predicted as

$$y_j(t) = \sum_{i=1}^{2} |L^1_{j,i}(\omega_i, \hat{e})|\hat{e}_i \sin\left(\omega_i t + \varphi_{e,i} + \angle\left(L^1_{j,i}(\omega_i, \hat{e})\right)\right) \quad (22)$$

with $L^1_{j,i}$ as in Theorem 3.1. Note that the HOSIDFs H^n of a CI can be computed using [13, Th. 3.1]. The resulting output signal is also portrayed in Fig. 6. It can be easily observed that the predicted signals do not correspond with the system output obtained from numerical simulation. This is because the effect of higher order harmonics is neglected in the output signal.

Next, we utilize Theorem 3.1 to compute the open-loop output. Note that P is Hurwitz. Furthermore, K_1 and K_2 are sinusoidal-input uniformly convergent [11, Prop. 2] and Assumption 2.1 holds for all u_i [11]. Therefore, the MIMO open-loop HOSIDFs of this system can be computed using (16) and (17) in Theorem 3.1. The magnitude and phase characteristics of the first five odd-order HOSIDFs are portrayed in Fig. 7. The even-order HOSIDFs have been omitted. Namely, the even-order HOSIDFs of a CI are all equal to zero, implying that the even-order open-loop HOSIDFs are also equal to zero. The solution to which the system's output converges can then be computed using (15). The resulting signal is visualized in Fig. 8, where the first five odd-order harmonics have been taken into account. The output signal is again compared with the one obtained numerically, which is also portrayed in Fig. 8. It can be concluded from the figure that the analytical result from Theorem 3.1 matches with the numerical result, validating Theorem 3.1.

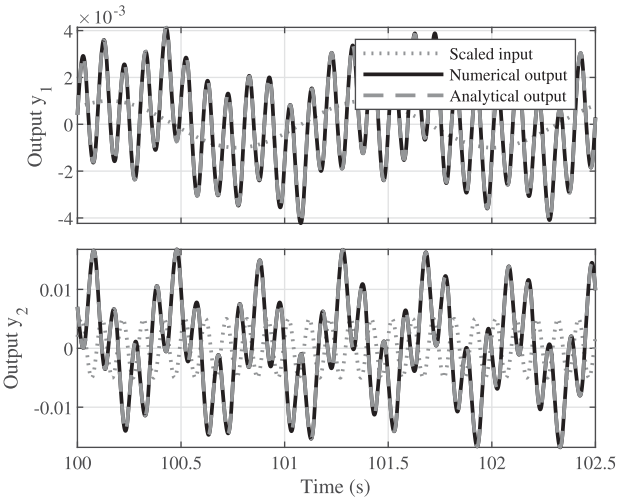

Fig. 8. Numerically computed system output compared to the analytical solution based on Theorem 3.1 ($k = 9$), for the considered example with P, K_1, and K_2, as in (18)–(20), and a sinusoidal input (21) with $\omega_1 = 0.81 \cdot 2\pi$, $\omega_2 = 10 \cdot 2\pi$, $\hat{e}_1 = 1$, $\hat{e}_2 = 10$, $\varphi_{e,1} = \frac{\pi}{4}$, and $\varphi_{e,2} = \frac{\pi}{8}$.

In this example, including the first five odd-order harmonics was sufficient for the analytical output to visually converge to the numerical output. Practically, one can use the HOSIDF's magnitude characteristics to determine the amount of harmonics that should be taken into account

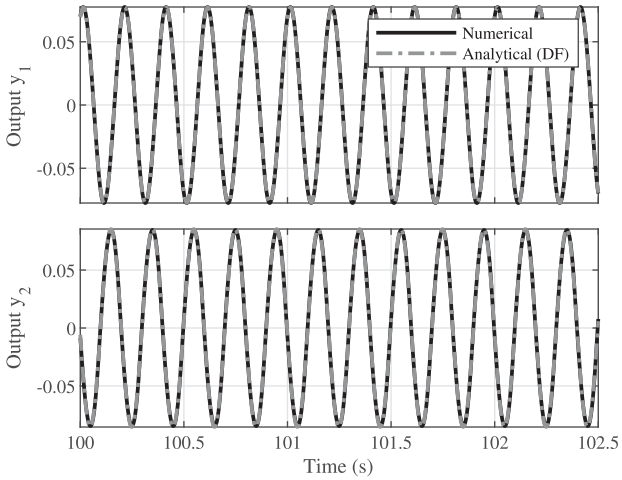

Fig. 9. Numerically computed system output compared to the analytical solution using the SIDF-method, for the considered example with P, K_1, and K_2, as in (18)–(20), and a sinusoidal input (21) with $\omega_1 = 5 \cdot 2\pi$, $\omega_2 = 5 \cdot 2\pi$, $\hat{e}_1 = 1$, $\hat{e}_2 = 10$, $\varphi_{e,1} = \frac{\pi}{4}$, and $\varphi_{e,2} = \frac{\pi}{8}$.

for an accurate prediction. One can observe in Fig. 7 that at the considered input frequencies, the magnitude generally decreases for higher order harmonics. When the magnitude of a harmonic is negligible compared with the (dominant) harmonic with the largest magnitude, its influence on the prediction also becomes negligible. It is important to note that the HOSIDF's magnitudes depend on the characteristics of the system under consideration, as well as the amplitudes and frequencies of the input sinusoids. Therefore, the amount of harmonics that should be taken into account depends on the use case.

B. Example II: Negligible Higher Order Harmonics

In this second example, we use the input frequencies $\omega_1 = 5 \cdot 2\pi$ and $\omega_2 = 5 \cdot 2\pi$. One can observe in Fig. 7 that the magnitude of the first-order harmonic is dominant over the other harmonics in all four input–output relations. This indicates that an accurate prediction can already be obtained based only on the first harmonic. The system output that is obtained from a numerical simulation is portrayed in Fig. 9, where it is compared to the output obtained from a first-order approximation using the SIDF. The figure shows that the first-order approximation indeed matches with the numerical result, which illustrates the potential of the developed MIMO HOSIDF method. Namely, it can be used as an intuitive tool to assess whether an SIDF-approximation is accurate or not.

V. Conclusion

In this article, output prediction methods are developed for a class of (open-loop) systems containing sinusoidal-input uniformly convergent elements in combination with various LTI elements around them. The prediction methods are based on a HOSIDF-analysis, which assumes that each of the input signals is sinusoidal. Theoretically, a fully accurate output prediction can be obtained when an infinite amount of higher order harmonics is taken into account. However, the considered example illustrates that an accurate prediction can already be obtained by taking only a few higher order harmonics into account. An important benefit of this method is the fact that it allows performance prediction based on a nonparametric model of the various LTI components, i.e., FRFs.

The developed prediction methods can be applied to a broad range of nonlinearities. Namely, all static nonlinearities—such as saturation, deadzone, ideal relays, and VGC—are sinusoidal-input uniformly convergent. The same holds for several dynamic nonlinearities, such as reset controllers and HIGS. In terms of application, the HOSIDFs can potentially be utilized in control design procedures, providing an intuitive frequency-domain based representation of the system. Namely, this has also been achieved with existing HOSIDF-methods in, e.g., [13] and [16].

As part of future work, we want to extend the HOSIDF-method toward closed-loop output prediction for systems containing sinusoidal-input uniformly convergent elements, while still being able to do this based purely on FRFs of the various LTI elements. Results into this direction have already been obtained for MIMO control systems with ideal relays in [21] and for SISO reset control systems in [13].

Acknowledgment

The authors would like to thank S. A. Hosseini and X. Zhang for proofreading the work.

Appendix
Technical Proofs

A. Proof of Lemma 3.1

Consider a SISO LTI element C_1 with any initial condition, which is subject to a sinusoidal input e as in (8). Then, if C_1 is Hurwitz, its output converges to a unique solution as in (3), with

$$\hat{r} = |C_1(j\omega)|\hat{e} \tag{23}$$

$$\varphi_r = \varphi_e + \angle C_1(j\omega). \tag{24}$$

Next, consider a SISO LTI element C_2 with any initial condition, which is subject to a sinusoidal input r as in (3), with (23) and (24). Then, if C_2 is Hurwitz, its output converges to a unique solution

$$w(t) = \hat{w}\sin(\omega t + \varphi_w) \tag{25}$$

$$\hat{w} = |C_2(j\omega)|\hat{r} \tag{26}$$

$$\varphi_w = \varphi_r + \angle C_2(j\omega). \tag{27}$$

Subsequently, consider a SISO NLTI element N with any initial condition, which is also subject to a sinusoidal input r as in (3), with (23) and (24). If N is sinusoidal-input uniformly convergent and Assumption 2.1 holds, then its output converges to a unique solution v as in (4), which can be rewritten into

$$v(t) = \hat{v}^0 + \sum_{n=0}^{\infty} v^n(t) \tag{28}$$

$$v^n(t) = \hat{v}^n \sin(n\omega t + \varphi_v^n) \tag{29}$$

$$\hat{v}^n = |H^n(\omega, \hat{r})|\hat{r} \tag{30}$$

$$\varphi_v^n = n\varphi_r + \angle H^n(\omega, \hat{r}). \tag{31}$$

From (25)–(31), it follows that signal $z := v + w$ converges to a unique solution:

$$z(t) = \hat{z}^0 + \sum_{n=1}^{\infty} z^n(t) \tag{32}$$

$$z^n(t) = \hat{z}^n \sin(n\omega t + \varphi_z^n) \tag{33}$$

$$\hat{z}^n = \begin{cases} |H^1(\omega, \hat{r}) + C_2(j\omega)|\hat{r}, & \text{for } n = 1 \\ \hat{v}^n, & \text{for } n \neq 1 \end{cases} \tag{34}$$

$$\varphi_{\mathrm{z}}^n = \begin{cases} \varphi_{\mathrm{r}} + \angle\left(H^1(\omega,\hat{r}) + C_2(j\omega)\right), & \text{for } n = 1 \\ \varphi_{\mathrm{v}}^n, & \text{for } n \neq 1. \end{cases} \tag{35}$$

Now, consider a SISO LTI element C_3 with any initial condition, which is subject to an input z as in (32)–(35). Then, if C_3 is Hurwitz, it follows from the superposition principle that the system output u converges to a unique solution:

$$u(t) = \hat{u}^0 + \sum_{n=1}^{\infty} u^n(t) \tag{36}$$

$$u^n(t) = \hat{u}^n \sin\left(n\omega t + \varphi_{\mathrm{u}}^n\right) \tag{37}$$

$$\hat{u}^n = |C_3(nj\omega)|\hat{z}^n \tag{38}$$

$$\varphi_{\mathrm{u}}^n = \varphi_{\mathrm{z}}^n + \angle C_3(nj\omega). \tag{39}$$

From (36) and (37), it can already be concluded that the unique solution is periodic with period $\frac{2\pi}{\omega}$. Furthermore, substituting (23), (30), and (34) in (38), and rewriting, yields

$$\hat{u}^n = \begin{cases} \left|C_3(nj\omega)\left[H^1(\omega,\hat{r}) + C_2(j\omega)\right]C_1(j\omega)\right|\hat{e} & \\ & \text{for } n = 1 \\ \left|C_3(nj\omega)H^n(\omega,\hat{r})C_1(j\omega)\right|\hat{e}, & \text{for } n \neq 1. \end{cases} \tag{40}$$

Similarly, substituting (24), (31), and (35) in (39), and rewriting, yields

$$\varphi_{\mathrm{u}}^n = \begin{cases} \varphi_{\mathrm{e}} + \angle\left(C_3(nj\omega)\left[H^1(\omega,\hat{r}) + C_2(j\omega)\right]C_1(j\omega)\right) & \\ & \text{for } n = 1 \\ n\left(\varphi_{\mathrm{e}} + \angle C_1(j\omega)\right) + \angle\left(C_3(nj\omega)H^n(\omega,\hat{r})\right) & \\ & \text{for } n \neq 1 \end{cases} \tag{41}$$

which, after some algebra, yields

$$\varphi_{\mathrm{u}}^n = \begin{cases} \varphi_{\mathrm{e}} + \angle\left(C_3(nj\omega)\left[H^1(\omega,\hat{r}) + C_2(j\omega)\right]C_1(j\omega)\right) & \\ & \text{for } n = 1 \\ n\varphi_{\mathrm{e}} + \angle\left(C_3(nj\omega)H^n(\omega,\hat{r})C_1(j\omega)\right) + \cdots & \\ \qquad (n-1)\angle C_1(j\omega), & \text{for } n \neq 1. \end{cases} \tag{42}$$

Finally, substituting (37), (40), and (42) in (36) yields the same expression as substituting (10) and (11) in (9), which concludes the proof.

B. Proof of Theorem 3.1

Consider a SISO NLTI element K_i with any initial condition, which is subject to a sinusoidal input $e_i(t) = \hat{e}_i \sin\left(\omega_i t + \varphi_{\mathrm{e},i}\right)$. Then, according to Lemma 3.1, if K_i is sinusoidal-input uniformly convergent and Assumption 2.1 holds, its output converges to a unique solution

$$u_i(t) = |K_i^0(\omega_i,\hat{e}_i)|\hat{e}_i + \cdots \sum_{n=1}^{\infty} |K_i^n(\omega_i,\hat{e}_i)|\hat{e}_i \sin\left(n(\omega_i t + \varphi_{\mathrm{e},i}) + \angle K_i^n(\omega_i,\hat{e}_i)\right). \tag{43}$$

Next, substituting (13) in (12), and rewriting, yields

$$Y_j(s) = \sum_{i=1}^{M} G_{j,i}(s) \quad \forall j \in [1, M] \tag{44}$$

$$G_{j,i}(s) = P_{j,i}(s)U_i(s). \tag{45}$$

Consider a SISO LTI plant $P_{j,i}$ that is Hurwitz and can have any initial condition. When applying an input u_i as in (43), by utilizing the superposition principle, we find that its output converges to a unique solution

$$g_{j,i}(t) = |P_{j,i}(0)||K_i^0(\omega_i,\hat{e}_i)|\hat{e}_i + \cdots \sum_{n=1}^{\infty} |P_{j,i}(nj\omega_i)||K_i^n(\omega_i,\hat{e}_i)|\hat{e}_i \cdot \ldots \sin\left(n(\omega_i t + \varphi_{\mathrm{e},i}) + \angle P_{j,i}(nj\omega_i) + \angle K_i^n(\omega_i,\hat{e}_i)\right) \tag{46}$$

$$g_{j,i}(t) = |P_{j,i}(0)K_i^0(\omega_i,\hat{e}_i)|\hat{e}_i + \cdots \sum_{n=1}^{\infty} |P_{j,i}(nj\omega_i)K_i^n(\omega_i,\hat{e}_i)|\hat{e}_i \cdot \ldots \sin\left(n(\omega_i t + \varphi_{\mathrm{e},i}) + \angle\left(P_{j,i}(nj\omega_i)K_i^n(\omega_i,\hat{e}_i)\right)\right). \tag{47}$$

Subsequently, utilizing (44), (47), and again the superposition principle, it can be observed that output y_j will converge to a unique solution given by

$$y_j(t) = \sum_{i=1}^{M}\Big[|P_{j,i}(0)K_i^0(\omega_i,\hat{e}_i)|\hat{e}_i + \cdots \sum_{n=1}^{\infty} |P_{j,i}(nj\omega_i)K_i^n(\omega_i,\hat{e}_i)|\hat{e}_i \cdot \ldots \sin\left(n(\omega_i t + \varphi_{\mathrm{e},i}) + \angle\left(P_{j,i}(nj\omega_i)K_i^n(\omega_i,\hat{e}_i)\right)\right)\Big]. \tag{48}$$

Finally, writing out (16) explicitly yields

$$L_{j,i}^n(\omega,\hat{e}) = P_{j,i}(nj\omega)K_i^n(\omega,\hat{e}_i). \tag{49}$$

Substituting (49) in (15) yields (48), which concludes the proof.

REFERENCES

[1] F. Lamnabhi-Lagarrigue et al., "Systems & control for the future of humanity, research agenda: Current and future roles, impact and grand challenges," *Annu. Rev. Control*, vol. 43, pp. 1–64, 2017.

[2] G. F. Franklin, J. D. Powell, and A. E. Emami-Naeini, *Feedback Control of Dynamic Systems*, 7th ed. London, U.K.: Pearson, 2015.

[3] R. Pintelon and J. Schoukens, *System Identification: A Frequency Domain Approach*, 2nd ed. Hoboken, NJ, USA: Wiley, 2012.

[4] J. Freudenberg, R. Middleton, and A. Stefanpoulou, "A survey of inherent design limitations," in *Proc. 2000 Amer. Control Conf.*, 2000, pp. 2987–3001.

[5] D. van Dinther, B. Sharif, S. J. A. M. van den Eijnden, H. Nijmeijer, M. F. Heertjes, and W. P. M. H. Heemels, "Overcoming performance limitations of linear control with hybrid integrator-gain systems," *IFAC-PapersOnLine*, vol. 54, no. 5, pp. 289–294, 2021.

[6] B. G. B. Hunnekens, N. van de Wouw, and D. Nešić, "Overcoming a fundamental time-domain performance limitation by nonlinear control," *Automatica*, vol. 67, pp. 277–281, 2016.

[7] G. Zhao, D. Nešić, Y. Tan, and C. Hua, "Overcoming overshoot performance limitations of linear systems with reset control," *Automatica*, vol. 101, pp. 27–35, 2019.

[8] M. Heertjes, N. Irigoyen, and D. Deenen, "Data-driven tuning of a hybrid integrator-gain system," *IFAC-PapersOnLine*, vol. 50, no. 1, pp. 10851–10856, 2017.

[9] S. A. Hosseini, M. S. Tavazoei, L. F. van Eijk, and S. H. HosseinNia, "Generalizing hybrid integrator-gain systems using fractional calculus," in *2022 IEEE Conf. Control Technol. Appl.*, 2022, pp. 1050–1055.

[10] M. F. Heertjes, "Variable gain motion control of wafer scanners," *IEEJ J. Ind. Appl.*, vol. 5, no. 2, pp. 90–100, 2016.

[11] Y. Guo, Y. Wang, and L. Xie, "Frequency-domain properties of reset systems with application in hard-disk-drive systems," *IEEE Trans. Control Syst. Technol.*, vol. 17, no. 6, pp. 1446–1453, Nov. 2009.

[12] A. Gelb and W. E. Vander Velde, *Multiple-Input Describing Functions and Nonlinear System Design*, 1st ed. New York, NY, USA: McGraw-Hill, 1968.

[13] N. Saikumar, K. Heinen, and S. H. HosseinNia, "Loop-shaping for reset control systems: A higher-order sinusoidal-input describing functions approach," *Control Eng. Pract.*, vol. 111, 2021, Art. no. 104808.

[14] P. W. J. M. Nuij, O. H. Bosgra, and M. Steinbuch, "Higher-order sinusoidal input describing functions for the analysis of non-linear systems with harmonic responses," *Mech. Syst. Signal Process.*, vol. 20, no. 8, pp. 1883–1904, 2006.

[15] P. Nuij, "Higher order sinusoidal input describing functions: Extending linear techniques towards non-linear systems analysis," Ph.D. dissertation, Eindhoven Univ. Technol., Eindhoven, The Netherlands, 2007.

[16] L. F. van Eijk, S. Beer, R. M. J. van Es, D. Kostić, and H. Nijmeijer, "Frequency-domain properties of the hybrid integrator-gain system and its application as a nonlinear lag filter," *IEEE Trans. Control Syst. Technol.*, vol. 31, no. 2, pp. 905–912, Mar. 2023.

[17] D. Rijlaarsdam, P. Nuij, J. Schoukens, and M. Steinbuch, "Spectral analysis of block structured nonlinear systems and higher order sinusoidal input describing functions," *Automatica*, vol. 47, no. 12, pp. 2684–2688, 2011.

[18] C. Cai, A. A. Dastjerdi, N. Saikumar, and S. H. HosseinNia, "The optimal sequence for reset controllers," in *2020 Eur. Control Conf.*, 2020, pp. 1826–1833.

[19] N. Karbasizadeh and S. H. HosseinNia, "Continuous reset element: Transient and steady-state analysis for precision motion systems," *Control Eng. Pract.*, vol. 126, 2022, Art. no. 105232.

[20] N. Karbasizadeh, A. A. Dastjerdi, N. Saikumar, and S. H. HosseinNia, "Band-passing nonlinearity in reset elements," *IEEE Trans. Control Syst. Technol.*, vol. 31, no. 1, pp. 333–343, Jan. 2023.

[21] A. Loh and V. Vasnani, "Necessary conditions for limit cycles in multiloop relay systems," *IEE Proc. - Control Theory Appl.*, vol. 141, pp. 163–168, May 1994.

[22] D. Rijlaarsdam, "Frequency domain based performance optimization of systems with static nonlinearities," Ph.D. dissertation, Eindhoven Univ. Technol., Eindhoven, The Netherlands, 2012.

[23] Y. Y. L. Chen, "Development of CRONE reset control," M. S. thesis, Delft Univ. Technol., Eindhoven, The Netherlands, Oct. 2017.

[24] J. C. Clegg, "A nonlinear integrator for servomechanisms," *Trans. Amer. Inst. Elect. Eng., Part II: Appl. Ind.*, vol. 77, no. 1, pp. 41–42, 1958.

[25] S. Skogestad and I. Postlethwaite, *Multivariable Feedback Control Analysis*, 2nd ed. Hoboken, NJ, USA: Wiley, 2005.